Thermal Effect of Er^{3+} Ions Embedded in Smart Nano-Composite Oxide Material Prepared by Sol-Gel Technique

I.K. Battisha[a,*], M.M.H. Ayoub[b], A.I. Hashem[c], E.H. Ahmed[b] and A. Amin[b]

[a]Solid State Physics Department, National Research Center (NRC), Giza, Egypt

[b]Polymers and Pigments Department, National Research Center (NRC), Giza, Egypt

[c]Chemistry Department, Ain Shams University, Egypt

(Received September 23, 2016; revised version April 3, 2017; in final form April 25, 2017)

The phosphosilicate for planar waveguides fabrication by using sol-gel, and particularly erbium-doped waveguide amplifiers, is reviewed. In particular, efforts to use sol-gel to improve molecular homogeneity in Er-doped phosphosilicate-based monolith and thin films will be discussed. A variety of material studies was carried out to investigate and optimize the sample preparation condition for such application. These include X-ray diffraction, the Fourier transform infrared and optical transmittance, absorption and refractive index calculation. The erbium nitrate precursors use is shown to alter the Er^{3+} ions doping in the prepared samples thermally treated in the final monolith glass form, in comparison to the use of thin film phosphosilicate sol-gel sample. Excess heat treatment is used to force prepared samples crystallization, moreover resulting photoluminescence analysis is used to detect the co-operative-up-conversion sample properties before and after heating.

DOI: 10.12693/APhysPolA.132.1277

PACS/topics: photonics, sol-gel, erbium ions, XRD, FESEM, HRTEM, optical refractive index

1. Introduction

The sol-gel method has been extensively investigated for the co-operative –up-conversion and optical waveguides fabrication, etc., where it is a convenient and flexible way to prepare monolithic samples and to deposit oxide films samples [1]. Co-operative-up-conversion processes in Er^{3+} ions-doped materials investigation has been of great interest since their first use as laser materials. This interest is due to the luminescence presence in the visible region, with a transition that can be enhanced by an appropriate host choice.

Other key application for sol-gel glass is photonics and/or integrated optics. A sol-gel is a feasible method for fabricating phosphosilicate components that can be used in communications fiber application. The sol-gel technique has now been used to make waveguides with low (< 0.3 dB/cm) propagation loss at the telecommunications wavelengths, especially 1550 nm [2, 3]. Sol-gel offers great performance possibilities, due to the ease of introducing a wide variety of dopants. Erbium ions, in particular, can provide amplification in the 1550 nm communications window through stimulated transitions from the $^4I_{13/2}$ metastable energy level to the ground state. Ions can be inverted to the metastable level by optical excitation via higher level; e.g. 980 nm is a suitable pump wavelength, and one at which laser diode sources are available at reasonably high power. For these reasons, erbium doped fiber amplifiers have become crucial components in long distance, high data-rate communication links. However, fiber amplifiers are bulky and expensive, and may these disadvantages can be reduced by planar integration. Homogeneity loss in these levels must be reduced, for keeping scattering losses low and to limit Er ion–ion interactions, which reduce gain such as co-operative up-conversion [4]. However, the solubility of erbium in silica alone is low for that we solved this problem in our work by doping the silica with phosphor ions which enhance the solubility of rare earth in the nanocomposite phosphosilicate monolith SPM.

Light source producing the optical signal is an important optical integrated circuit (OIC) component, optical waveguide systems transmit and can process this optical signal, then detector will convert the optical signal back to the electric domain giving rise to ease and low-cost production techniques. Then the light propagation processing can transmit the light from one point to another using optical waveguide systems [5–9].

The development of nanocomposite phosphosilicate doped with Er^{3+} ions and sintered at different temperature to study the thermal treatment influence on it were present in this work, aiming to prepare the system to can be used successfully in the near future for wave guide application. The nanocomposite samples structure, optical, co-operative–up-conversion and morphology will be elucidating.

2. Experimental

Phosphosilicates nanocomposite containing 20 mol.% phosphate; (SiO_2–20 mol.% P_2O_5) S20P were prepared in monolithic and thin film forms symbolic S20PM and

*corresponding author; e-mail: szbasha@yahoo.com

S20PT at different sintering temperature 60, 500, 700, and 900 °C. Constant Er^{3+} ions molar percent was embedded in the prepared S20P and S20PT sample at 2.5 mol.% symbolic as [S20P2.5ErM] and [S20P2.5ErT], respectively. Hydrolysis and poly condensation reaction of tetra-ethoxysilane $(CH_3CH_2OH)_4$-Si (TEOS), (TEOS, 99.999%, Sigma–Aldrich) as SiO_2 precursor and triethylphosphate as P_2O_5 precursor in ethanol (CH_3CH_2OH) solutions were carried out. A pre-hydrolysis reaction of (SiO_2:20 mol.% P_2O_5) solution was allowed under vigorous stirring at room temperature for long time using distilled water (H_2O), however ethanol and HCl were used as solvent and catalyst, respectively. These solutions were then filtered before performed as thin film and monolith. The final used mixture solutions were homogeneous, transparent and no precipitates appeared.

2.1. Monolith samples preparation

After mixing the starting precursor materials monomers first undergo hydrolysis reactions to give (Si–OH), (Si–O–Si),(P–OH) and/or (P–O–Si) functional groups in the first step. The silica gel modification can be achieved via the particular molecule reaction with either the siloxane (nucleophilic substitution at the Si) or silanol (direct reaction with the hydroxyl group) functions [10, 11]. Doping the silica gel with 20 mol.% phosphate consisting of these new functional groups (Si–O–Si), (P–O–P) and (P–O–Si) which are formed by condensation reactions between Si–OH, Si–OR, P–OR and P–OH groups. The Er^{3+} ions were introduced in the process, by dissolving Er $(NO_3)_3$–H_2O, solution in the preceding precursors with different molar ratios, respectively.

The resultant solutions were kept in closed glass vials and/or square plastic boxes during the gelation process which starts at the moment giving the hydrolyzed species in the mixture. All samples were aged for 21 days at 60 °C, where the samples were in the transition states from low viscosity (liquid) to the intermediate viscosity (gel) by evaporating the solvent molecules before drying.

2.2. Thin film samples preparation

The same homogeneous resultant solutions were used for thin film preparation. The prepared nanocomposite solutions were dropped and dispersed on quartz silica substrates and glass substrates. The solutions then, allowed to spun at 3500 rev./min for 30 s by using a homemade spin coater. At least two successive coatings were required to provide suitable effective film thickness. The film samples were dried for 30 min and then heated at different temperature at 500, 700, 800 and 900 °C for 3 h, giving cracks free, homogeneous, clear and transparent thin films suitable for photonic application such as planar optical waveguide system (PWGS).

2.3. Characterization

The prepared samples X-ray diffraction (XRD) patterns were recorded with an X-ray diffractometer using monochromatized Cu K_α radiation of wavelength = 1.54056 Å. Crystallite sizes G were determined from the Scherrer equation

$$G = K\lambda/D\cos\theta,$$

where K is the Scherrer constant (0.9), λ is the wavelength, and D is the full width (in radians) of the peak at half maximum intensity (FWHM). The value of G was confirmed by using the U-fit program. Figure 1 shows the XRD patterns of the S20P2.5M (A) dried at 60 °C for three weeks and (B) sintered for three hours at two different temperature 500 and 900 °C. The results indicate that sample remained amorphous at 60 °C, where as previously reported by our team work that the condensations process kinetics cannot be increased at this sintering temperature [12, 13]. The crystallinity began at 500 °C due to the phosphor ions presence and it increases with the annealing temperature increase from 14 up to 22 nm at 500 and 900 °C, respectively. This increase might be due to the surface densification as a result of the OH and the OR groups removal from the surface.

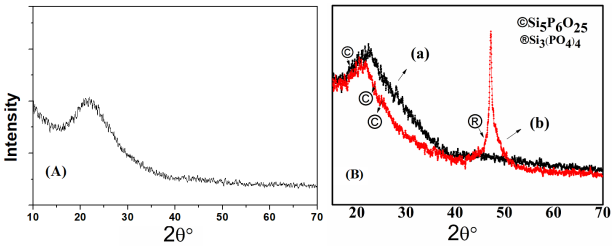

Fig. 1. XRD diffraction of SP2.5ErM at (A) 60 °C and (B) at two different temperatures (a) 500 °C and (b) 900 °C, respectively.

The peak at 2θ equal to 47° corresponding to monoclinic silica phosphate SiP_2O_7 phase was detected. These results are compatible with the previously reported [4–7] that the P_2O_5 presence into the silicate network leads to the host materials crystallization enhancement. However the P_2O_5 presence improves the solubility of RE such as Er^{3+} ions doped sol-gel process, thereby improving its dispersion and reduce the ion–ion interactions possibility in Er^{3+}-rich phase which tends to form in phosphosilicate systems [14, 15].

This finding was reported by our team work previously [12, 13] where we suggested that when the (Er^{3+} and Yb^{3+}) ions are embedded in the silica-phosphate and then subjected to thermal treatment for densification, the structure of the prepared materials changes due to most properties change of the gel in the host skeleton which is attributed to the Si–O and P–O bonds cross-linking development due to dehydration poly- condensation of the system.

Rare earth oxides and related compounds are in so small quantities that they might not appear with their corresponding X-ray diffraction patterns.

FTIR spectra were recorded on JASCO, FTIR, 6100, made in Japan by using KBr pellets. Nearly normal transmittance and reflectance spectra were done

by Jasco V-570 spectrophotometer, in wavelength range (0.2–2.5 µm). The refractive indexes n for all investigated samples are calculated.

The high resolution transmission electron microscope (HRTEM) analysis has been made using a high resolution JEOL JEM-2100 equipment operating at 120 kV with attached CCD camera.

The coarse and fine microstructures and the morphology of the prepared samples were depicted by using high resolution field emission gun quanta FEG 250 scanning electron microscope (HRSEM). The FESEM gives information on the surface morphology of the sample, which can helps us check whether the growth has taken place or not. The film thickness was measure from FESEM.

The spectrophotometer Model V-570 UV/VIS/NIR was used to measure the transmittance and the absorption spectrum. The instrument specified by resolution 0.1 nm and wavelength accuracy ±0.3 nm (at a spectral bandwidth of 0.5 nm) in the UV/VIS region. The refractive index can be expressed in terms of n according to the Fresnel equation

$$n = \frac{1+R}{1-R} + \sqrt{\frac{4R}{(1-R)^2} - K^2}.$$

The photoluminescence spectra were obtained using Jasco FP-777 or 6500 Japan spectrofluorometer. The light source is xenon arc lamp 150 W.

The photoluminescence spectra are obtained using Jasco FP-6500 Japan spectrofluorometer. The light source is xenon arc lamp 150 W, the step was 0.5 nm, the excitation slit bandwidth was 5 nm and the emission slit bandwidth was 5 nm.

3. Results and discussion

Figure 2a–c shows the S20P2.5ErM surface morphology using the HRSEM micrographs, sintered at different temperatures: (a) 60, (b) 500 and (c) 900 °C, respectively. It is noted that the monolithic prepared samples exhibited nearly the same arrangement structure with long-range ordered structures. The increase in temperature from 60 up to 900 °C has no influence on these ordered structures. While for comparison between the three temperatures at constant magnification during the densification process increase, the system rearrangements appeared indicated more agglomeration appearance at higher temperature as a result of increase of the samples densification at higher temperature specially at 900 °C. The obtained results might be attributed to the large interstitial voids appearance and large particles distributed over the monolithic gel at lower temperature, while by increasing its temperature more agglomeration occurred.

For thin film samples S20P2.5ErT sintered at 2 different temperatures 500 and 900 °C shown in Fig. 3, nearly the same homogeneous surface was observed even at lower temperature 500 °C, very small agglomeration degree can be detected. At higher temperature 900 °C the film surface appeared more homogeneous, denser film

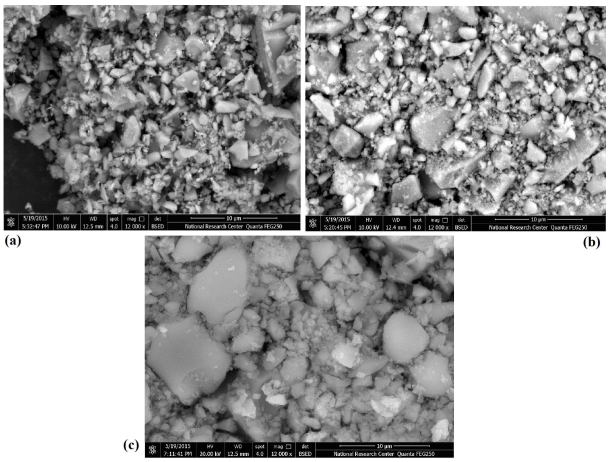

Fig. 2. SP2.5ErM FESEM sintered at (a) 60 °C, (b) 500 °C, (c) at 900 °C, respectively.

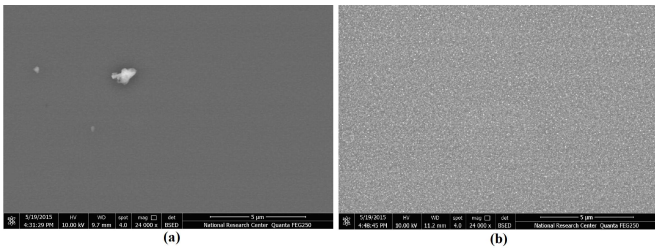

Fig. 3. SP2.5ErT FESEM sintered at different temperatures: (a) 500 °C and (b) 900 °C, respectively.

with good uniformity was obtained. This may be attributed to densification as OH and OR groups' removal result from the surface at higher temperature as reported in XRD and FTIR parts in this work.

From the comparison between the two form samples monolith S20P2.5ErM and thin film S20P2.5ErT sintered at 500 and 900 °C, it is clearly seen that the roughness and coarse scale are lower in thin film than monolith one. The films have smaller pores, which imply that it is denser. Moreover the films seem to be more homogeneous than monolith prepared samples.

The FTIR spectra for the pure phosphosilicate samples S20PM sintered at (a) 500 and (b) 900 °C for 3 h is shown in Fig. 4, while the monolithic sample SP2.5ErM dried at (a) 60 °C for 3 weeks and then sintered at different temperature (b) 500 °C, (c) 700 °C and (d) 900 °C for 3 h is shown in Fig. 5.

Three main bands, characteristic of the phosphosilicate glasses, are observed in Fig. 4, the band near 1336 cm^{-1} sintered at 500 °C for 3 h is mainly due to the phosphate network asymmetric stretching of P = O bonds [10, 16]. The mentioned peak was very small and broad at lower temperature, while it appeared well at 900 °C for pure S20PM and S20P2.5ErM with small shift to lower wave number after the addition of erbium ions. The strong peak at about 1083 cm^{-1} was assigned to the silica and phosphor bridging oxygen atoms. The mentioned peak at about 1083 cm^{-1} shifted to higher wave number near 1100 cm^{-1} at higher temperature in pure S20PM and be-

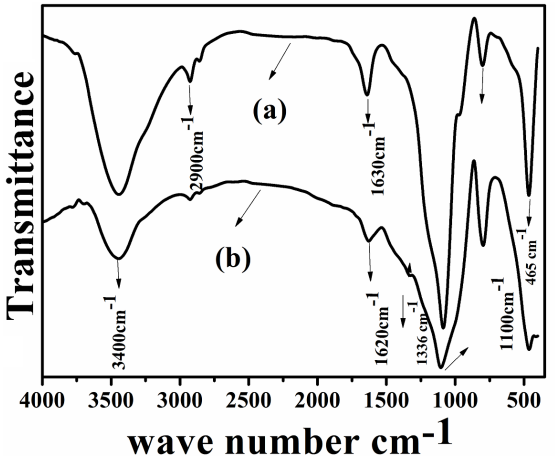

Fig. 4. S20PM FTIR spectra sintered at two different temperatures: (a) 500 °C and (b) 900 °C, respectively.

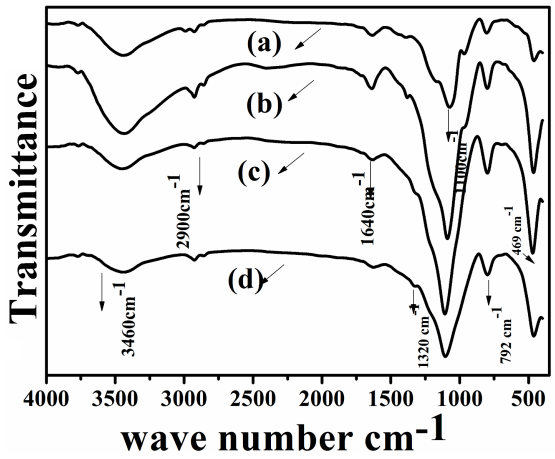

Fig. 5. SP2.5ErM FTIR spectra SP2.5ErM sintered at different temperatures: (a) 60 °C, (b) 500 °C, (c) 700 °C and (*d*) 900 °C, respectively.

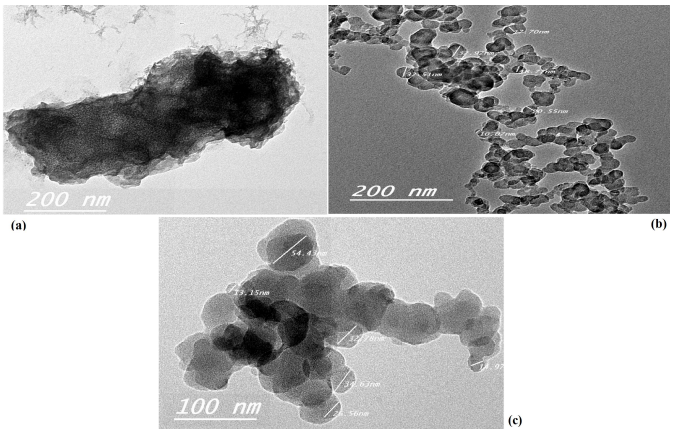

Fig. 6. SP2.5ErM FETEM SP2.5ErM sintered at (a) 60 °C, (b) 900 °C, respectively, both at constant magnification 200 nm, while (c) 500 °C at magnification 100 nm to prove the crystallite size (CS) values.

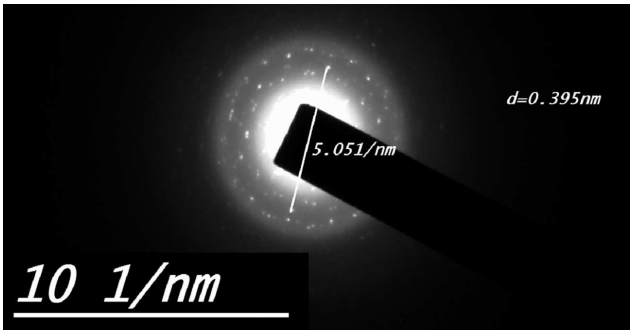

Fig. 7. SP2.5ErM FETEM diffraction pattern.

come broader and decreased in intensity, Fig. 4. Moreover, 1083 cm^{-1} peak increases in intensity and shifted to higher wave number at higher temperature as an effect of doping with Er^{3+} ions as shown in Fig. 5, due to the rearrangement of the S20PM structure after the Er^{3+} ions addition. The shoulder near 970 cm^{-1} is due to P–O tetrahedral with one P = O bond (11). In fact the more complete densification of samples after increase of the temperature up to 900 °C causes the decrease in this shoulder intensity while it disappears at 900 °C for S20PM and S20PxErM at 900 °C, Figs. 6 and 7, due to the groups attached to the P atom total electron negativity. The host pure phosphosilicate contain PO_3-tetrahedral units series connected by three oxygen bridging. The Si–O–Si symmetric stretching is observed around 800 cm^{-1} for all samples pure and doped with Er^{3+} ions, which increases in intensity and shifted to lower wave number by increasing the temperature up to 900 °C.

The S20PM host material can be explained in Q^n distribution terms, where n is the bridging oxygen numbers. Q is equal to isolated tetrahedra (orthophosphate groups), Q^1 corresponds to the end groups (pyrophosphate), Q^2 is due to middle groups (metaphosphate) and Q^3 to branching groups (ultraphosphate). By adding the P_2O_5, homogeneous disruption in silica gel occurs and the modifier oxide cations occupy interstitial positions. Generally, the phosphate asymmetric and symmetric stretching vibrations presented in SP demonstrated on Q^1 and Q^2 groups [17].

The 465 cm^{-1} absorption band attributed to Si–O–Si bending oxygen atoms vibration perpendicular to the Si–O–Si plane and the tetrahedral SiO_4 ring structure, shifted to 468 cm^{-1} higher wave number as an OH groups elimination result from the silica gel due the temperature increase up to 900 °C [18–20].

The hygroscopic character of the phosphate glasses is confirmed by the absorptions bands due to O–H groups observed in the range 4000–1500 cm^{-1}. The wide band starting from 3750 to 3250 cm^{-1} is due to the δ (O–H) groups symmetric stretching and δ (H–O–H). The δ (O–H) groups deformation modes and absorbed water molecules, δ (H–O–H) were found at 1630 cm^{-1}, which can interact through hydrogen bonds with silanol groups resulting in a lower intensity for the monolith sample sintered at 900 °C. Both bands located between 3750 and

3250 cm^{-1} and at 1638 cm^{-1} decreased in intensity by increase of the temperature and become wider, but they still appear even at such higher temperature 900 °C [21]. At 900 °C the OH bands intensities have considerably diminished [22]. It is well known that the higher porosity in the sol-gel glasses which allows accommodating water molecules caused the formation of clusters aggregation during the sol-gel growth process. The silanol groups are formed on the surface by two main processes [20]. First they are formed in the course of silica synthesis, e.g. during the condensation polymerization of $Si(OH)_4$. Secondly, surface OH groups can be formed as a result of de-hydroxylated silica rehydroxylation when it is treated with water or aqueous solutions. While the silanol groups is responsible of a surface hydrophilic at a sufficient concentration [20].

It has to be noted that C–H groups stretching is present at 2900 cm^{-1} in the prepared samples. It is attributed to the υ (P–OH) groups stretching vibration and ethyl molecules, it shifted to higher wave number at about 2937 cm^{-1} by increase of the temperature up to 900 °C [23, 24]. Moreover its intensity decreases by increasing the temperature, where the first υ (Si–OH) and υ (P–OH) condensation groups leads to υ as (P–O–P links) and υ as (Si–O–Si).

As shown in Fig. 5 for S20P2.5ErM sintered at 900 °C the mentioned peak at 2900 cm^{-1} increases in intensity as a function of temperature at 500 °C and then it decreases at higher temperature 700 and 900 °C.

The increasing temperature effects from 60 up to 900 °C on the S20PE2.5M particle sizes and shape are investigated by using the high resolution transmission electron microscopy (HRTEM) as shown in Fig. 6a–c for different temperature 60, 500, and 900 °C. The synthesized samples particle shapes are irregular and relatively aggregated molecules at 500 and 900 °C, while amorphous phases appeared at lower temperature 60 °C. It displayed nanostructure scale at 900 °C, the particles became uniform with spherical shape, homogeneous and well-dispersed erbium ions in prepared host nanocomposites at these two temperature. Some agglomerations degree was present in the clusters, which increase at 900 °C.

The calculated average particle size from FETEM was found to be equal to about 21 and 22 nm at 500 and 900 °C, respectively for S20PE2.5M prepared sample. The obtained crystallite sizes from FETEM are nearly compatible with the obtained XRD results at 500 and 900 °C, respectively. An important effect on the densification processes was achieved by well particle size distribution. Nanostructure phase and a narrow size distribution aid in obtaining dense and homogeneous materials [25, 26], these results are compatible with the observed FTIR data.

The particle size measured from HRTEM micrographs is somewhat different from the value obtained from XRD data, which is quite common in other materials [27]. Figure 7 shows the HRTEM selected-area electron diffraction (SAED) pattern of SP2.5ErM sintered in air for 3 h at 900 °C. An observable and strong SAED patterns give information about the nanoscale composition in the samples structure and that the d spacing is equal to 0.395 nm at 900 °C.

The refractive index linearly increased as shown in Fig. 8 with increasing silica-phosphate glass density as that revealed in normal multi-component glasses [28, 29]. The silicate network combination with phosphate as a dopant changes fundamentally the silicate glass properties, where the depolymerization of the phosphate cation occurs, thus diminishing the silicate glass network cross-linking to create a more open structure [29]. The higher phosphate content at 20 mol.% gives greater disorder in the silicate network and this displays an enhancement in the refractive index values especially with increase of the temperature. The silica-phosphate glass refractive index values decreased at higher hydroxyl impurity content occurred at 500 °C. The phosphate ions concentration increases the contribution in the silica-phosphate system depolymerization which enhances the increase in the concentration of bonding defects and NBOs in the silicate network [28–30]. The refractive indexes n values for SP2.5ErM are given at constant wavelength = 1400 nm was found to be equal to 1.6 and 1.74 at 500 and 900 °C, respectively. The obtained result implying that an increase in n values is associated with the material densification and condensation. The obtained data allow the low loss coupling systems planar waveguide preparation [31].

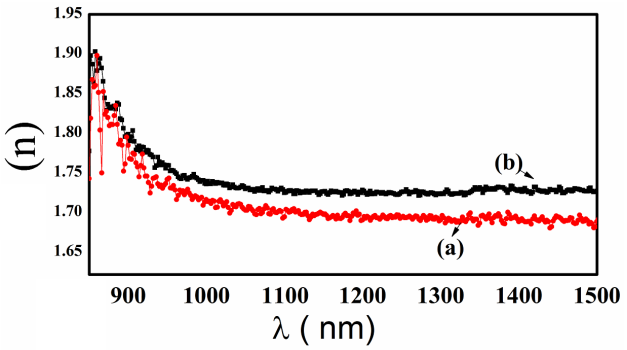

Fig. 8. Optical refractive index n for SP2.5ErT sintered at (a) 500 °C and (b) 900 °C, respectively.

The exciting source effect on the monolithic SP2.5ErM and thin film SP2.5ErT samples using the laser diodes with excitation at 850 nm is presented in Fig. 9a–d. The figures show the room temperature co-operative upconversion spectra for the two sample forms sintered at two different temperatures 500 and 900 °C. The emission bands observed at 511 and 525 nm are attributed to the intra-$4f$ transitions $^2H_{11/2} \rightarrow^4 I_{15/2}$ while the group emission bands in the range between 530 and 600 nm are attributed to another green intra-$4f$ transitions $^4S_{15/2} \rightarrow^4 I_{15/2}$. It is clearly seen that the thin film intensities are lower than the monolith, this may be due to the big difference in thickness and structure between them. Increase of the thermal treatment causes a de-

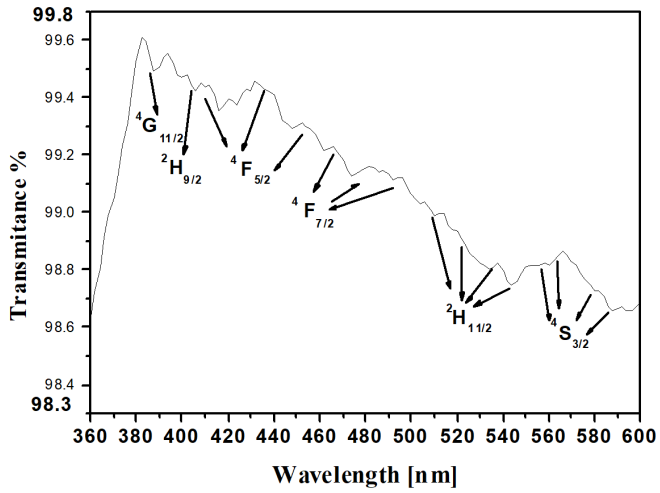

Fig. 9. SP2.5ErT transmission spectrum sintered at 500 °C.

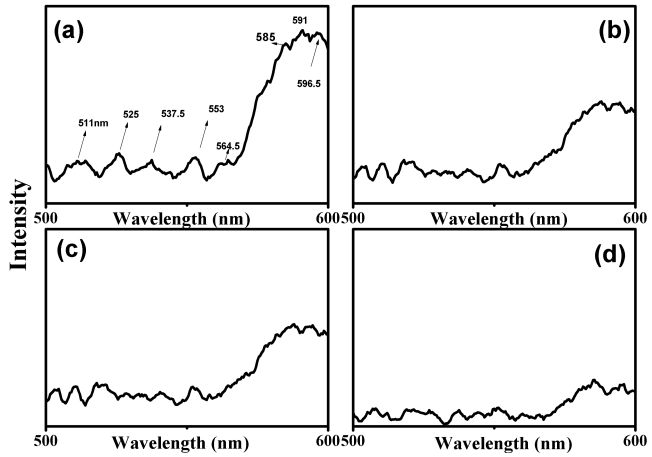

Fig. 10. RT co-operative–up-conversion emission spectra for SP2.5ErM (a,b) and SP2.5ErT (c,d), both sintered at 500 °C (a,c) and 900 °C (b,d), respectively.

fects concentration to decrease followed by decrease of the bands intensity. However at 900 °C for both sample forms a quenching process appears. The emission is induced by defects, where the pores disappear, hydroxyl content decreases and the nanocomposite density increases affecting the co-operative-up-conversion emission spectra [26, 32].

The UV-Vis SP2.5ErT transmission spectrum prepared sample sintered at 500 °C in the wavelength ranging from 360 up to 600 nm is shown in Fig. 10. The obtained transmission spectrum confirmed good transparency for SP2.5ErT that was higher than 98.6%. The obtained spectrum is erbium ions energy level $^4I_{15/2}$ (ground state) to the erbium ions excited states $^4G_{3/2}$, $^2H_{9/2}$, $^4F_{5/2}$, $^4F_{7/2}$, $^4H_{11/2}$ and $^4S_{3/2}$ to $^4I_{15/2}$. In addition by focusing on the green region we can observe the erbium ions energy level $^4H_{11/2}$ and $^4S_{3/2} \rightarrow ^4 I_{15/2}$ which confirm the cooperative -up-conversion-emission presence seen in Fig. 9 [33].

4. Summary and conclusion

Nanocomposite sol-gel pure phosphosilicate S20PM and doped with 2.5 mol.% of Er^{3+} ions in monolith and thin film forms SP2.5ErM and SP2.5ErT, respectively with good adherence to quartz substrate using alkoxides as precursor were successfully prepared. FTIR analyses indicated the chemical bonds in the monolith samples. The increase in temperature causes an increase in the crystallite sizes, the peak intensities and new phases appeared. Using the Scherrer formula confirmed with the win fit program we obtained the following crystallite sizes values; 14 and 22 nm for the S20P2.5 ErM sample sintered at 500 and 900 °C, respectively implying the nanostructure phase consisting the nanocomposites prepared samples. The data were confirmed using HRTEM nearly the same crystallite sizes obtained from XRD patterns were obtained from HRTEM giving rise to the following values 21 and 22 nm for the samples sintered at 500 and 900 °C, respectively. From FESEM it is clearly seen that the roughness and coarse scale are lower in thin film than monolith samples. The films have smaller pores, which imply its denser nature. The films seem to be more homogeneous than monolith prepared samples. By studying the co-operative-up-conversion for the SP2.5ErM and SP2.5ErT sample forms green emission bands observed at 511 and 525 nm are attributed to the intra-$4f$ transitions $^2H_{11/2} \rightarrow ^4 I_{15/2}$ while the group green emission bands in the range between 530 and 600 nm are attributed to another green intra-$4f$ transitions $^4S_{15/2} \rightarrow ^4 I_{15/2}$.

After succeeding in controlling more the preparation conditions and the nanocomposite prepared samples properties, new work will be done in the near future now to optimize the preparation condition to be ready for planer wave guide applications materials. Moreover more analyses such as the Raman and photoluminescence in wider wavelength region will be contributed.

Acknowledgments

The authors acknowledge the team work of the Italian-Egyptian sharing project entitled “Smart optical nanostructures for green photonics”, 2013–2017.

References

[1] V.R. Almeida, Q. Xu, C.A. Barrios, M. Lipson, *Opt. Lett.* **29**, 120 (2004).

[2] I.K. Battisha, A. El Nahrawy, *New J. Glass Ceram.* **2**, 17 (2012).

[3] M. Kamal, I.K. Battisha, M.A. Salem, A.M.S. El Nahrawy, *J. Sol-Gel Sci. Technol.* **58**, 507 (2011).

[4] R.G. Hunsperger, *Integrated Optics Theory and Technology*, 6th ed., Springer, 2009, Ch. 1.

[5] V. Zabelin, L.A. Dunbar Le, N. Thomas, R. Houndre, *Opt. Lett.* **32**, 53 (2007).

[6] D.H. Kwon, D.H. Werner, *Opt. Expr.* **16**, 18731 (2008).

[7] G.L. Vossler, C.J. Brooks, K.A. Winik, *Electron. Lett.* **31**, 1162 (1995).

[8] A. Lukowiak, A. Chiappini, A. Chiasera, D. Ristic, I. Vasilchenko, C. Armellini, A. Carpentiero, S. Varas, G. Speranza, S. Taccheo, S. Pelli, I.K. Battisha, G.C. Righini, W. Strek, M. Ferrari, *J. Opt. Quant. Electron.* **47**, 117 (2015).

[9] A. Lukowiak, R.J. Wiglusz, A. Chiappini, C.Armellini, I.K. Battisha, G.C. Righini, M. Ferrari, *J. Non-Cryst. Sol.* **401**, 32 (2014).

[10] Y. Song, C. Bian, Yang Li, J. Tong, S. Xi, *J. Biomed. Sci.* **05**, (2016).

[11] R.M. Almeida, J.D. Mackenzie, *J. Non-Cryst. Solids* **40**, 535 (1980).

[12] Y. Badr, I.K. Battisha, M. Kamal, A.M.S. El-Nahrawy, *New J. Glass Ceram.* **1**, 69 (2011).

[13] I.K. Battisha, A. El Beyally, S.L. Soliman, A.M.S. Nahrawi, *New J. Glass Ceram.* **6**, 62890 (2016).

[14] A.J. Silversmith, N.T.T. Nguyen, B.W. Sullivan, D.M. Boye, C. Ortiz, K.R. Hoffman, *J. Lumin.* **128**, 931 (2008).

[15] M. Szumera, I. Wacławska, *J. Therm. Anal. Calorim.* **88**, 151 (2007).

[16] H.C. Vasconcelos, *J. Sol-Gel Sci. Technol.* **55**, 126 (2010).

[17] C. Daniela, M. David Pickup, C. Jonathan Knowles, I. Ahmed, M.E. Smith, J.R. Newport, *J. Non-Cryst. Solids* **353**, 1759 (2007).

[18] M. Rokta, W. Mozgawa, M. Handke, *J. Mol. Struct.* **596**, 171 (2001).

[19] H.S. Costa, M.F. Rocha, G.I. Andrade, E.F. Barbosa Stancioli, M.M. Pereira, R.L. Orefice, W.L. Vasconcelos, H.S. Mansur, *J. Mater. Sci.* **43**, 494 (2008).

[20] L.T. Zhuravlev, *Coll. Surf. A Physicochem. Eng. Asp.* **173**, 1 (2000).

[21] I.K. Battisha, H.H. Afify, M. Ibrahim, *J. Magn. Magn. Mater.* **306**, 211 (2006).

[22] C. Coelho, F. Babonneau, T. Aza, L. Bonhomme Coury, J. Maquet, G. Laurent, C. Bonhomme, *J. Sol-Gel Sci. Technol.* **40**, 181 (2006).

[23] T. Uma, M. Nogami, *Fuel Cells* **7**, 279 (2007).

[24] J.C. Brinker, W.G. Scherert, *Sol-Gel Science*, Academic, New York 1990.

[25] I.A. Rahman, P. Vejayakumaran, C.S. Sipaut, J. Ismail, M. Abu Bakar, R. Adnan, C.K. Chee, *Coll. Surf. A Physico-Chem. Eng. Asp.* **294**, 102 (2007).

[26] I.K. Battisha, H.H Afify, Y. Badr, *J. Sol–Gel Sci. Techn.* **25**, 5 (2002).

[27] S. Kundoo, A.N. Banerjee, P. Saha, K.K. Chattopadhyay, *Mater. Lett.* **57**, 2193 (2003).

[28] H. Neumann, W. Horig, E. Reccius, H. Sobotta, B. Schumann, G. Kuhn, *Thin Solid Films* **61**, 13 (1979).

[29] E.T.Y. Lee, E.R.M. Taylor, *Opt. Mater.* **27**, 323 (2004).

[30] M. Abdel-Baki, F. El-Diasty, *J. Curr. Opin. Solid State Mater. Sci.* **10**, 217 (2006).

[31] E.T.Y. Lee, E.R.M. Taylor, *J. Opt. Mater.* **27**, 323 (2004).

[32] A. Chiasera, I. Vasilchenko, D. Dorosz, M. Cotti, S. Varas, E. Lacob, G. Speranza, A. Vaccari, S. Valligatla, L. Zur, A. Lukowiak, G.C. Righini, M. Ferrari, *J. Opt. Mater.* **63**, 153 (2017).

[33] I.K. Battisha, *J. Non-Cryst. Solids* **353**, 1748 (2007).